Vol. 6 • No. 6 • March 22 • 2017

www.advhealthmat.de

# ADVANCED HEALTHCARE MATERIALS

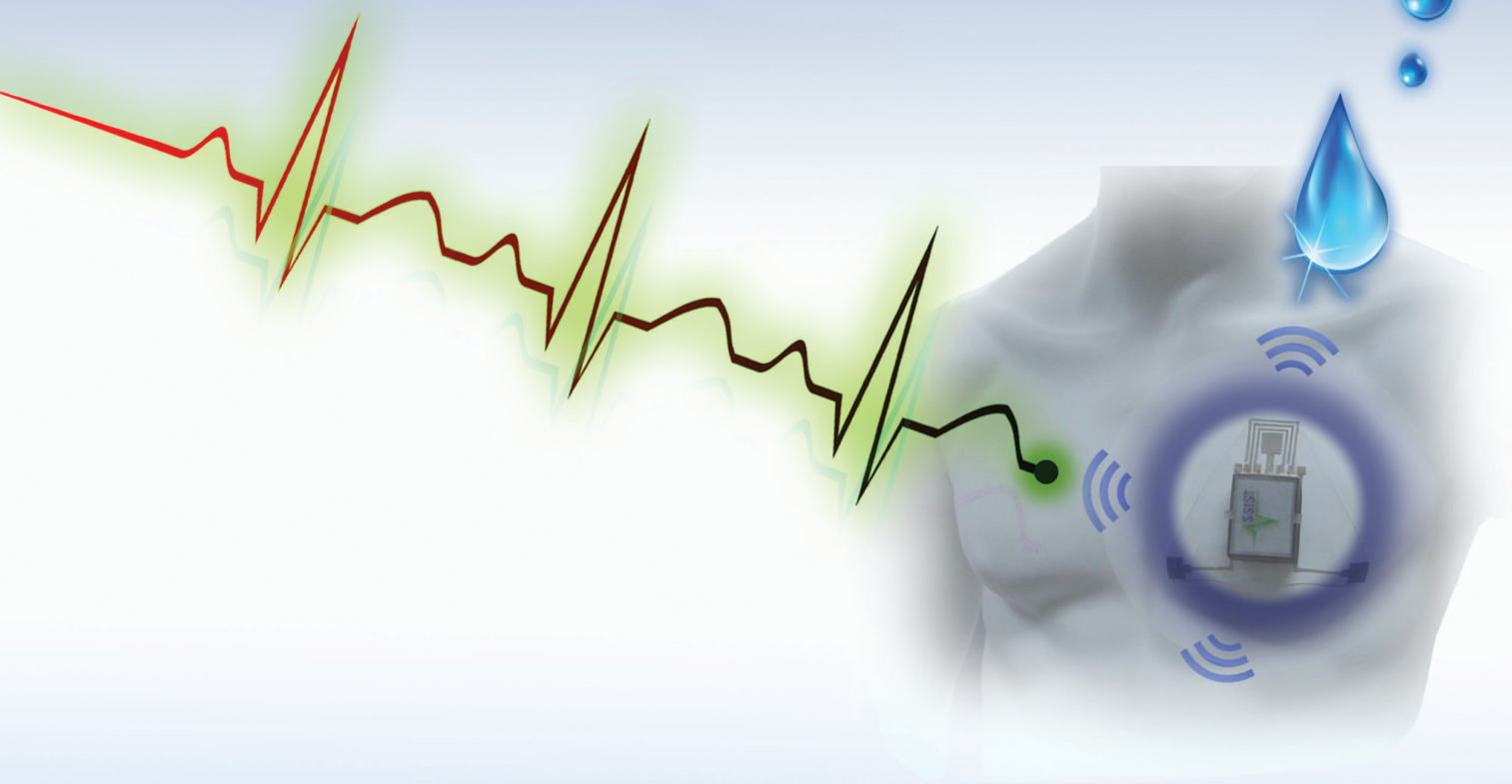

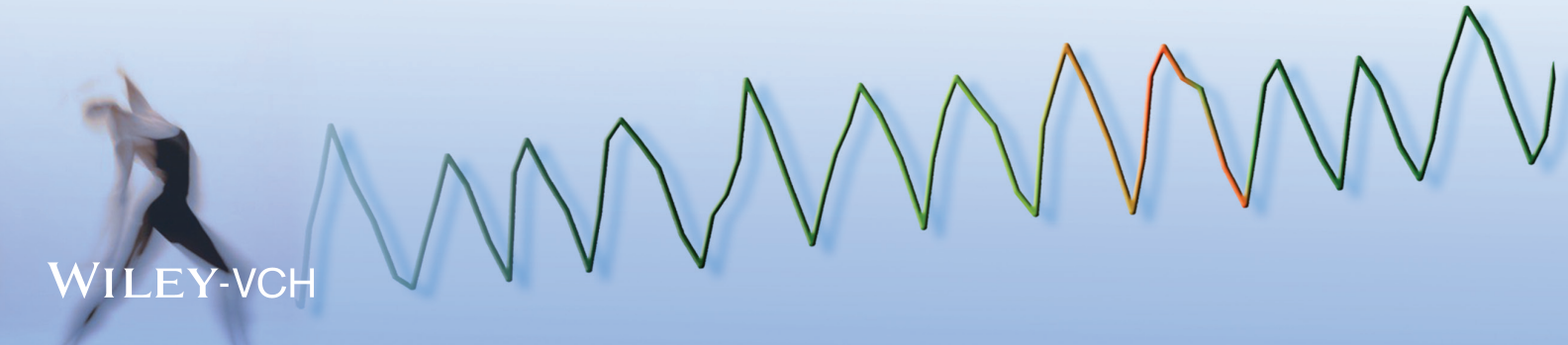

WILEY-VCH

# A Wearable Hydration Sensor with Conformal Nanowire Electrodes

*Shanshan Yao, Amanda Myers, Abhishek Malhotra, Feiyan Lin, Alper Bozkurt, John F. Muth,* and Yong Zhu**

**A wearable skin hydration sensor in the form of a capacitor is demonstrated based on skin impedance measurement. The capacitor consists of two interdigitated or parallel electrodes that are made of silver nanowires (AgNWs) in a polydimethylsiloxane (PDMS) matrix. The flexible and stretchable nature of the AgNW/PDMS electrode allows conformal contact to the skin. The hydration sensor is insensitive to the external humidity change and is calibrated against a commercial skin hydration system on an artificial skin over a wide hydration range. The hydration sensor is packaged into a flexible wristband, together with a network analyzer chip, a button cell battery, and an ultralow power microprocessor with Bluetooth. In addition, a chest patch consisting of a strain sensor, three electrocardiography electrodes, and a skin hydration sensor is developed for multimodal sensing. The wearable wristband and chest patch may be used for low-cost, wireless, and continuous monitoring of skin hydration and other health parameters.**

## 1. Introduction

Hydration of the body is an important physiological parameter to measure, but is challenging to measure accurately. For example, high-performance athletes would like to know more about their hydration state since this can be directly linked to athletic performance. Such knowledge is also of interest to workers such as first responders who may dehydrate when working in extreme conditions. It is a well-known problem that when coaches start training young athletes for American football in the summer, and when the military starts physically training recruits that dehydration and heat stroke pose serious risks.

Many methods to assess dehydration are qualitative, for example, by accessing how the person looks (e.g., sunken eyes and cracked lips), or by examining the volume and color of urine. More quantitative assessment relies on measuring change in hydration by weighing a naked person before and after exercise, or by using instruments that measure the physical properties of the skin such as conductance, capacitance, impedance, thermal conductivity, and reflectance of optical or electromagnetic radiation.[1–4] Almost all of these measurements are taken in clinical settings.

To replace the expensive, bulky instruments and achieve low-cost, long-term hydration monitoring, hydration sensors that are mechanically compliant and can form a conformal contact with the skin are a significant technological advance. The mechanical compliance can facilitate the long-term wearability of the sensors, and allows for spatially mapping the electronic properties of the skin by using an array of sensors.[5] Ultrathin "electronic tattoo"[6,7] is a representative example, which adopts the top-down approach (i.e., patterning followed by transfer printing) to enable high-performance stretchable electronics.

In this paper, we report a low-cost and stretchable hydration sensor that is built up from bottom-up synthesized silver nanowires (AgNWs) inlaid in a polydimethylsiloxane (PDMS) matrix. The compliant, stretchable AgNW/PDMS electrode provides a conformal electrical/mechanical interface to the skin and can be worn continuously to monitor the skin hydration based on the skin impedance method. The fabrication process is simple and scalable to large areas. By integrating the hydration sensor with other electronic components (e.g., for data acquisition and wireless communication), two wearable form factors, a wristband for skin hydration monitoring and a multifunctional chest patch for concurrent sensing of strain, electrocardiography (ECG), and hydration were demonstrated.

## 2. Results and Discussion

### 2.1. Sensor Fabrication and Sensing Mechanism

The skin hydration sensors were developed based on our previously demonstrated highly stretchable and conductive AgNW conductors, in which AgNWs were embedded just below the surface of PDMS. Due to the superior conductivity of silver and the mechanical robustness of nanomaterials and polymers, stretchable conductors which can maintain good conductivity at highly strained state (conductivity of ≈5000 S $cm^{-1}$ at 50%

Dr. S. Yao, A. Myers, Prof. Y. Zhu
Department of Mechanical and Aerospace Engineering
North Carolina State University
Raleigh, NC 27695, USA
E-mail: yong_zhu@ncsu.edu
A. Malhotra, F. Lin, Prof. A. Bozkurt, Prof. J. F. Muth
Department of Electrical and Computer Engineering
North Carolina State University
Raleigh, NC 27695, USA
E-mail: muth@ncsu.edu

DOI: 10.1002/adhm.201601159

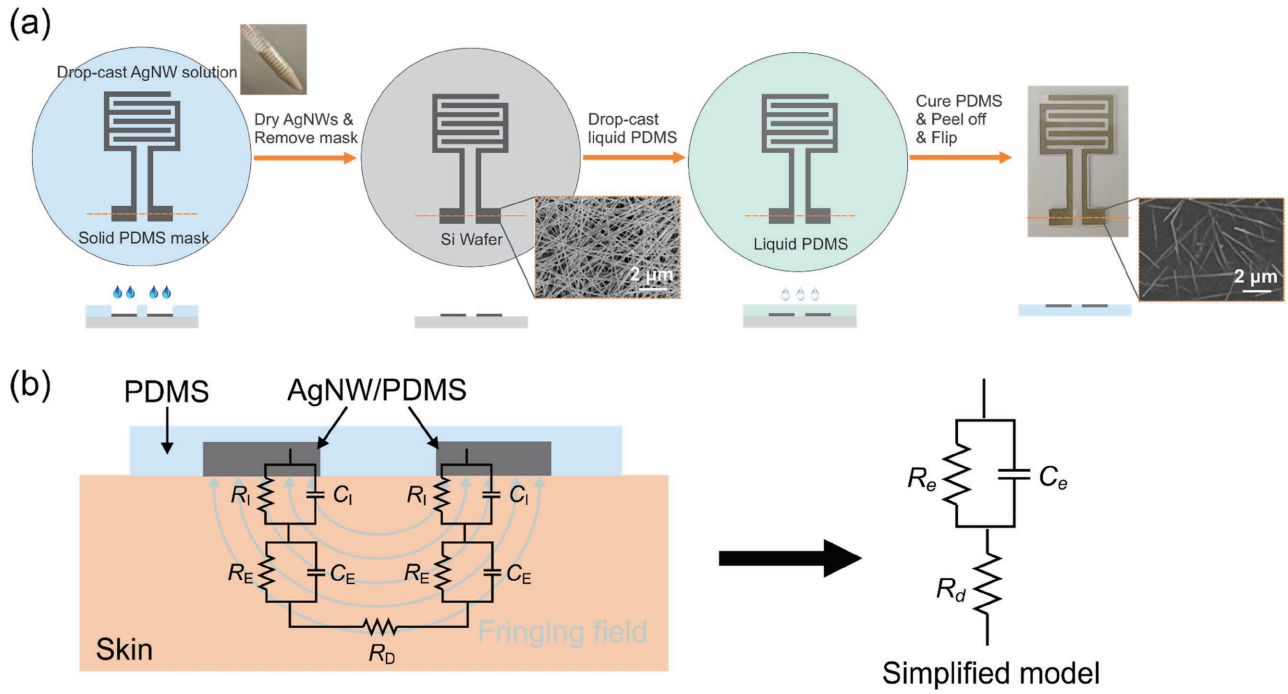


**Figure 1.** a) Fabrication process of the AgNW sensor. The left SEM image shows the AgNW conductive network before being embedded into the PDMS matrix. The right SEM image shows the surface of the AgNW/PDMS electrode. The exposed nanowires provide surface conductivity while the remaining nanowires are embedded in the PDMS. Scale bars: 2 μm. b) Schematic illustration of the AgNW sensor placed onto the skin with the fringing field penetrating the upper layer of skin, the equivalent electrode–skin model, and the simplified model.

tensile strain) were achieved.[8,9] The AgNW-based skin hydration sensor was fabricated following the procedure reported previously,[8,10] as shown in **Figure 1**a. The AgNWs were cast in an interdigitated pattern with finger length of 20 mm and spacing of 2 mm and then embedded just below the surface of PDMS to form two stretchable, interdigitated electrodes. The two electrodes act as a capacitor that can be used to measure skin hydration. Interdigitated patterns were chosen to maximize the interaction between the two electrodes within a small area. The two contact pads are used to connect the hydration sensor to other circuit components. The resulting hydration sensor is stretchable and mechanically/electrically robust, which allows for long-term use. In addition, the flexible and stretchable nature of the electrode enables conformal contact with the surface of the skin that is generally rough.

Skin impedance is a commonly used method to measure skin hydration[11] and is achieved by placing two electrodes on the surface of the skin. The fringing field between the two electrodes penetrates the upper layer of skin, as schematically shown in Figure 1b. The skin impedance measured by the two electrodes can be electrically modeled using a series of capacitors and resistors. The contact interface between electrode and the skin surface can be described by a resistor $R_I$ in parallel with a capacitor $C_I$, which is dependent on applied pressure and the humidity of the skin.[12,13] The epidermis is modeled by a parallel circuit consisting of a capacitor $C_E$ and a resistor $R_E$. The dermis and underlying subcutaneous tissues, mainly composed of blood vessels, nerves, preparatory glands, and hair follicles, exhibit a pure resistive behavior and can be modeled by a resistor $R_D$. Due to symmetry of the two electrodes, the equivalent circuit can be approximated as a parallelly connected resistor $R_e$ and capacitor $C_e$ arising from the electrode–skin contact interface and epidermis, in series with a resistor $R_d$ from the dermis and the underlying tissue.[14] Increasing the water content of the skin increases the conductivity and the dielectric constant of the skin by providing more conductive pathways.[13,14] The decreased contact impedance and decreased impedance from the epidermis result in a decrease of the measured skin impedance as a function of skin hydration level. Schwan[15] showed the dielectric relaxation responses of skin at various alternating current frequencies. At low frequencies, 0.1–1000 Hz, the dielectric response is mainly due to the top most layer of skin, the stratum corneum. Since we are more interested in the hydration level of epidermis, the sensing frequency started from 10 kHz to avoid the influence of the topmost layer of skin. The highest sensing frequency was set to be 100 kHz due to the limit of the maximum working frequency (100 kHz) of the AD5933 network analyzer. The chosen working frequency range for the reported skin hydration sensors (10–100 kHz) is comparable to that used in the literature.[16]

### 2.2. Sensor Characterization

The skin hydration sensors were characterized by three different tests to evaluate the effect of the ambient hydration or humidity, and the skin hydration using both artificial skin and human skin. In other words, we investigated the sensor response to external (ambient) and internal (physiological) water content.

The first test investigated the effect of the ambient relative humidity on the skin impedance of the hydration sensor. Artificial skin with similar electrical properties to the upper layers of human skin was fabricated according to Ito et al.[17] and optimized for low-frequency sensing following the compound ratios outlined by Yamamoto et al.[18] The artificial skin served as a control in the sense that its own water content remained constant throughout the test to ensure that any change in the measured impedance was a result of the varying external humidity. The hydration sensor was placed on the artificial skin and inserted into a humidity chamber. The humidity was lowered to 20% relative humidity by flooding the chamber with nitrogen gas. From there, the intake of nitrogen was adjusted to allow the humidity to slowly increase over a period of ≈60 min, which allowed the humidity levels to stabilize at each interval while being fast enough to prevent any water evaporation from the artificial skin. An impedance measurement at 10 kHz was recorded at a 5% humidity increase interval. At ≈45% relative humidity, a bubbler was used to continue increasing the humidity up to 100% relative humidity. During the test, the temperature of the humidity chamber was 20 ± 0.5 °C. The results, depicted in **Figure 2**a, show a 0.62% change in impedance readings with increasing relative humidity levels. This indicates that the skin hydration sensor can give stable readings regardless of the external environment of the wearer. It also demonstrates the robust contact of the hydration sensor with the skin. Slow absorption of water vapor into PDMS over a long time could affect the impedance reading. To mitigate this effect, three possible ways could be explored in the future study: (1) modifying the permeability of PDMS by modifying the structure,[19] (2) modifying the surface of PDMS, for example, using a thin coating of water impermeable material,[20] and (3) in addition to the active impedance sensor, employing a dummy impedance sensor that has a thin coating on the surface of AgNW/PDMS to avoid direct electrical contact with skin but otherwise is identical to the active impedance sensor.[16]

The second test investigated the effect of the internal water content, or the skin hydration level, on the skin impedance using an artificial skin as a control. This test also served as a calibration of the AgNW skin hydration sensor against a commercially available hydration meter (DelfinTech MoistureMeterD) (Figure 2b). The MoistureMeterD (MMD) implemented rigid open-ended coaxial probes, as indicated in Figure 2b, to measure the dielectric constant of the skin relative to that of the air; the hydration level is indicated using the relative dielectric constant.[21] The use of the artificial skin allows precise control of the skin hydration level over a wide range.

The artificial skin was prepared to be in a highly hydrated state. As the water inside the artificial skin evaporated with the help of a hair dryer, the hydration was measured using both the MMD and the AgNW hydration sensor. As expected, the impedance measured by the AgNW sensor increased as the water content of the artificial skin decreased, which was correlated with the decrease in the reading of the MMD (Figure 2c). The relationship between the impedance measured at 100 kHz and the MMD reading follows an exponential relationship, as shown in Figure 2d. Then Echem Analyst software (Gamry Instruments) was employed to extract the equivalent circuit model parameters of skin impedance. We found that with the current electrode design and sensing frequency, $R_e$ and $C_e$ play a major role while the value of $R_d$ does not change much in the resulting skin impedance, indicating the fact that the change

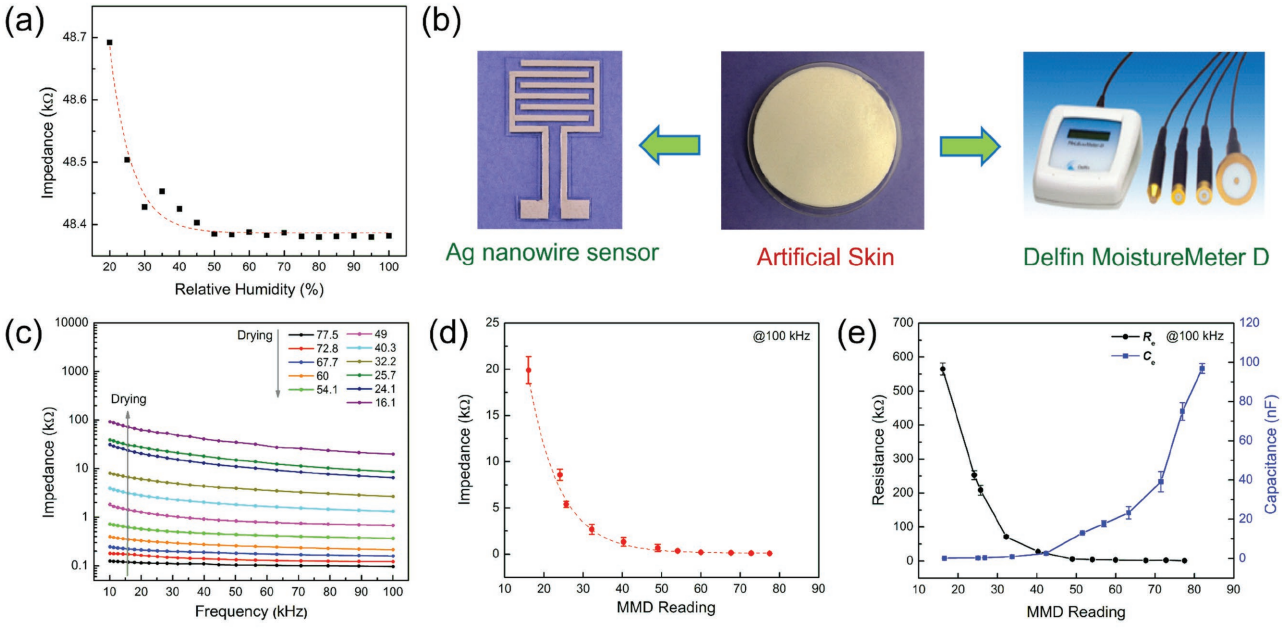


**Figure 2.** a) Impedance values measured from AgNW sensor on artificial skin at 10 kHz as a function of increasing humidity. b) The calibration was conducted on artificial skin between the AgNW sensor and a commercial moisture meter MoistureMeterD (MMD). c) Skin impedance measured from AgNW sensor between 10 and 100 kHz and the corresponding MMD readings as the artificial skin dries. d) Comparison of skin impedance measured from AgNW sensor at 100 kHz and MMD readings. e) Extracted equivalent circuit model parameters ($R_e$, $C_e$) as a function of MMD readings. d,e) Results presented were averaged from three experiments and expressed as the mean ± SD.

in the measured skin impedance is mainly due to the hydration level change in epidermis. For this reason, only the fitted values of $R_e$ and $C_e$ were summarized, as shown in Figure 2e. $R_e$ decreases while $C_e$ increases with the increase in the hydration level as a result of improved electrode–skin contact and increased conductivity and dielectric constant of skin.

Finally, the AgNW sensor was tested for human skin (**Figure 3**a). Skin lotion was applied on the skin of the forearm for 5 min to increase the skin hydration level and then the excess lotion on the skin was removed. Due to the moisturizing effect, a significant drop in skin impedance was observed in the initial reading after applying lotion (Figure 3b,c), corresponding to an increase in skin hydration. The skin impedance slowly recovered with time and fully recovered to the value before applying lotion after 20 min. Consistently, $R_e$ showed a similar trend with skin impedance and $C_e$ showed an opposite trend, which is consistent with the previous analysis (Figure 3d).

### 2.3. Wristband for Skin Hydration Monitoring

The wristband was chosen as the first form factor due to the good user acceptance of wearing wristwatch like devices, although the sensor can also be integrated into an armband, a chest strap, or a headband. A small-scale, low power circuit was designed to acquire the signals and transmit the data wirelessly via Bluetooth communication. The printed circuit board (PCB) layout and block diagram of the personal hydration monitor are shown in **Figure 4**a. The principle components were chosen to realize the desired functions at low power. The impedance was measured using a high precision impedance converter chip AD 5933 (Analog Devices) that combines an on-board frequency generator with an analog-to-digital converter (ADC). A microcontroller CC2541 (Texas Instruments) offers a power-optimized system on chip solution for low-power Bluetooth, with an industry standard 8051 microcontroller, 256 kilobytes in-system programmable flash memory, and 8 kB random access memory. Impedance measurements on the same AgNW interdigitated sensor were performed using both the AD5933 network analyzer and a desktop impedance analyzer (HP Agilent 4392A), sweeping the frequency from 10 to 100 kHz. The measured impedances using AD5933 controlled by the CC2541 microcontroller and the HP Agilent 4392A showed good agreement (Figure 4b). This indicates that the AD5933 impedance converter system is viable as a portable alternative to standard desktop impedance analyzers.

As shown in Figure 4c,d, a PCB containing the network analyzer chip (AD5933), the ultralow power microprocessor with Bluetooth radio (CC2541), and a button cell battery was connected to the AgNW sensor, using micro coaxial cables and rubber epoxy that allow the connection to remain secure while still retaining the stretchable nature of the electrode. A 3D printed spacer was used to enable secure contact between the AgNW sensor and the skin, and isolate the sensing component from the electrical circuit. The PCB, spacer, and electrode were secured and worn on the body using an iPod Nano wristband,

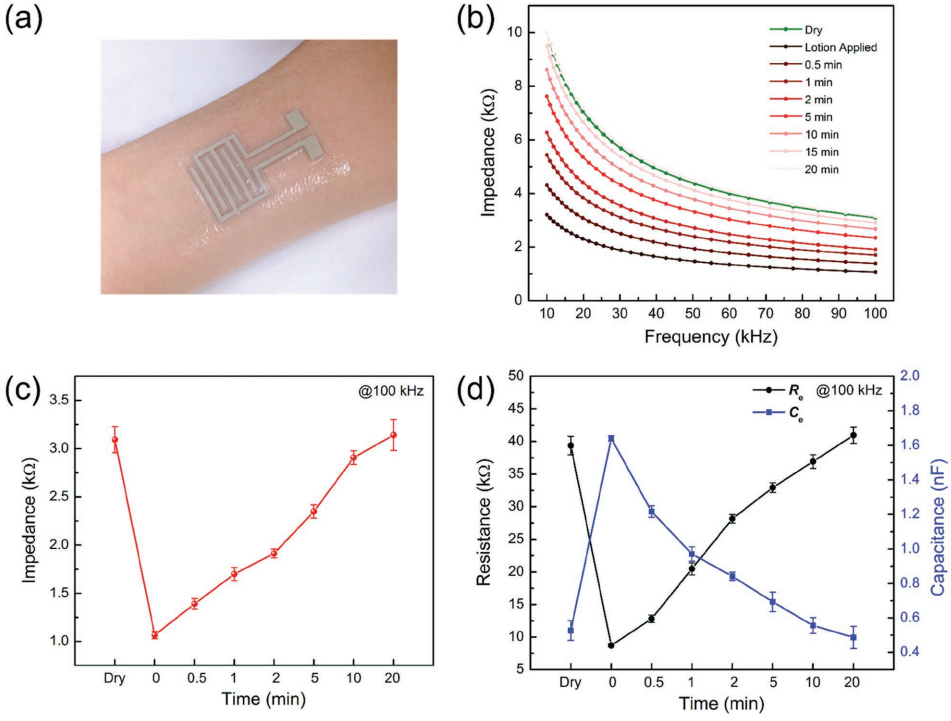


**Figure 3.** a) Photograph showing the AgNW sensor placed on the inner side of forearm. b) The measured impedance change between 10 and 100 kHz from human skin before (dry) and after applying lotion. c) Comparison of skin impedance measured from AgNW sensor at 100 kHz before (dry), and after applying lotion. d) Extracted equivalent circuit model parameters ($R_e$, $C_e$) before (dry) and after applying lotion. c,d) Results presented were averaged from three experiments and expressed as the mean ± SD.

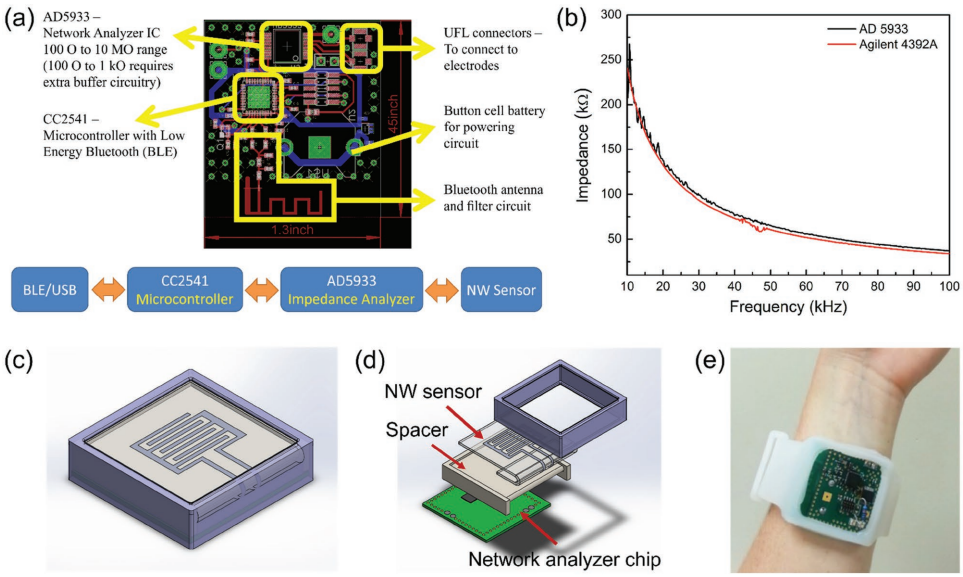


**Figure 4.** a) PCB layout (top) and block diagram (bottom) of system. b) Comparison of the impedance measurement from the AgNW sensor on the artificial skin between a desktop impedance analyzer (HP Agilent) and the portable evaluation board. c) CAD rendering of the assembled portable hydration monitor. d) Exploded view showing the PCB, 3D printed spacer, AgNW electrode, and encasing. Note that the flexible electrode allows the top surface contacts to be folded over to make contact with the printed circuit board contacts. e) The hydration monitor as worn on the wrist like a watch.

as the dimensions of the personal hydration monitor and the iPod Nano are identical. Figure 4e shows the assembled system as worn on the wrist.

### 2.4. Chest Patch for Multimodal Sensing

Dehydration can be a risk factor, the cause or symptoms of various diseases, such as kidney stone diseases, skin diseases, gastroenteritis, diabetes, respiratory infections, and heart diseases.[22–24] To better track the personal health parameters and monitor the related diseases, multimodal sensing in addition to the hydration sensing is needed. To demonstrate the application of the hydration sensor for multimodal sensing, a multifunctional sensor patch using the chest patch form factor was developed.

In view that ECG is a powerful tool in diagnosing and treatment of cardiovascular diseases, central nervous system disorders, electrolyte imbalances, lung diseases, and other conditions[25] and the fact that cardiovascular disease is one of the main cause of death, ECG sensing is included to monitor the heart activity and access the heart rate during workout. Continuous ECG monitoring in a wearable form factor could significantly cut down the cost and personnel load on healthcare. The commonly used gel electrode, however, cannot be used in a long-term, continuous setting due to the skin irritation caused by the gel and signal degradation as the gel dehydrates. The highly conductive and stretchable AgNW/PDMS dry electrode eliminates the use of the conductive gel but maintains compliant contact with the skin, which allows for high signal quality and enables long-term, continuous ECG monitoring.[26]

Dehydration often occurs during exercise and training. It would be beneficial to monitor the hydration level and track the activities simultaneously. A highly stretchable capacitive strain sensor[27] was also incorporated in the chest patch to track the skin strain, due to the following two reasons: (1) Together with the heart rate from ECG, the strain associated with human motions during workout can be used to analyze the intensity of the activities and prevent dehydration; (2) Since the ECG signals collected under motion are typically noisy, the strain signals may be correlated with the ECG signals and has the potential to mitigate the motion artifacts in ECG signals. In addition, while demonstrated for skin hydration sensing, the skin impedance measurement also has the potential to be used for the tracking of other health parameters. For example, excursions of glucose levels can change the electrolyte balance in blood, surrounding cells, and interstitial fluids, resulting in a change in the dielectric spectrum.[28,29] Emotional arousal levels affect the sweat gland activity, and hence change the skin conductance response.[30,31] Hence, various physiological parameters relevant to the wellness can be correlated to skin impedance.

The sensor layout and sensing concept of the chest patch are given in **Figure 5**a,b. To achieve a compact layout and facilitate the connection, the configuration of two parallel strips was adopted as the hydration sensor instead of the interdigitated pattern as used previously. Three square-shaped AgNW/PDMS electrodes at the corners of the chest patch serve as the ECG electrodes, two adjacent parallel AgNW/PDMS strips around the top ECG electrode are used to record the skin impedance, and a three-layer capacitive structure comprising two strips of AgNW/Dragon Skin conductors with a dielectric layer (Ecoflex 0010) in between acts as the strain sensor.[27] A self-adhesive substrate was used to attach the patch to skin.[32] The capacitive strain sensor was calibrated using a tensile stage to record the relative capacitive change as a function of tensile strain up to 100%. The demonstrated strain range is far beyond that of traditional thin film based strain gage (typically 5%) and sufficient for detecting the strain associated with human motions. The

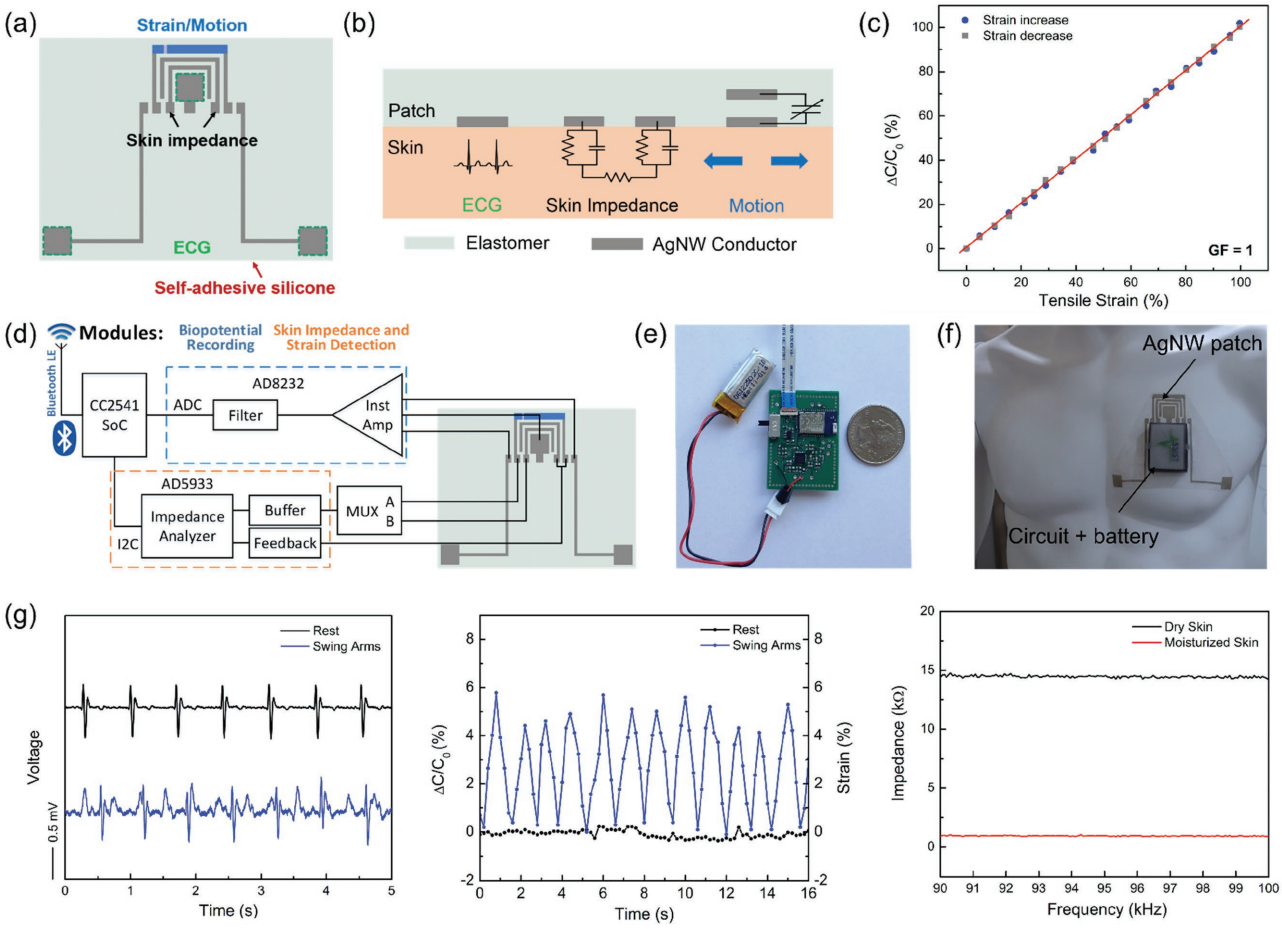


**Figure 5.** a) Layout of the patch including three ECG electrodes (boxed), a strain sensor, and an impedance sensor. b) Schematic illustration of the sensing concept. c) Relative capacitance changes as a function of applied tensile strain. d) Block diagram of the interface circuit. e) Actual populated printed circuit board. f) Integrated chest patch with circuit board and battery enclosed in a 3D printed box self-adhering to the chest of a mannequin. g) Multimodal data obtained from chest: ECG signals under rest and motion; skin strain associated with swinging arms and skin impedance before and after applying lotion.

gage factor of the strain sensor, defined as the relative capacitive change divided by the mechanical stain is 1 (Figure 5c).

ECG recording was achieved using Analog Devices AD8232 heart rate monitor front end with three-lead configuration for optimal signal detection. Since both skin impedance and strain can be detected and deduced from impedance spectroscopy, both sensing elements shared an Analog Devices AD5933 impedance converter in order to minimize overall size of the circuit. A circuit board with Texas Instruments Bluetooth Low Energy microcontroller CC2541 was used for wireless transmission to a nearby data aggregator (Figure 5d). The final size of the PCB board was 2.5 × 3.5 $cm^2$ (Figure 5e). The PCB, sensor patch connected on the PCB using a flexible flat cable (FFC), and a rechargeable Li-ion polymer battery were packed in a 3D printed box that can be directly mounted on top of the sensor patch (Figure 5f). When the circuit is powered by a rechargeable 1.48 Wh Li-ion polymer battery, it can operate up to 37 h with power consumption of 40 mW. The multifunctional chest patch was able to simultaneously detect the ECG under rest and under motion, the skin strain associated with body motion, and the skin hydration change. The initial testing results are shown in Figure 5g, which demonstrated the feasibility of recoding multiple health parameters using the multimodal sensors. Motion artifacts are clearly seen from the ECG signals obtained under motion. Study is currently underway to correlate the ECG motion artifacts with the strain signals as a potential way to mitigate the motion artifacts. The multimodal sensing and correlation of the data give a more comprehensive understanding of the body conditions and will greatly facilitate the tracking of wellness and the treatment of illness.

## 3. Conclusions

A wearable AgNW based skin hydration sensor was fabricated and calibrated with respect to external humidity change and internal skin water content change. Results showed that the sensor is insensitive to external humidity change and the skin impedance decreases with the increase in skin hydration level due to the increase in skin conductivity and dielectric constant. The wearable, low-cost hydration sensor compared well with the MMD commercial instrument. Two wearable form factors,

a wristband for skin hydration sensing and a multifunctional chest patch composed of strain sensor, ECG electrode, and skin hydration sensor were demonstrated. While the present hydration sensor was designed to measure hydration in the epidermis, the spacing of the electrodes, and the operating frequency can be adjusted to measure hydration in other skin layers.[11,33] This noninvasive, low-cost, wearable, and wireless system has potentials to help detect dehydration among athletes, military personnel, and the elderly, provide insight into athletic performance and other physiological parameters, assist the cosmetic scientists for the development of moisturizers, and benefit the diagnosis of skin diseases.

## 4. Experimental Section

*Fabrication Process of AgNW/PDMS Skin Hydration Sensor*: The fabrication process of the AgNW/PDMS skin hydration sensor is schematically illustrated in Figure 1a. Liquid PDMS (Sylgard 184, Dow Corning) with the weight ratio of "base" to "curing agent" of 10:1 was cast onto a Si substrate, degassed in a vacuum chamber, and cured at 60 °C for 2 h. The cured PDMS was patterned into an interdigitated shape with finger length of 20 mm and spacing of 2 mm. AgNWs in ethanol (SLV-NW-90, Blue Nano) with average length of 10 µm and diameter of 90 nm were drop-cast into the area defined by the mask. The AgNWs were subjected to baking at temperature of 50 °C for 10 min to evaporate the solvent (ethanol). After removing the PDMS mask, AgNW patterns were formed on the substrate. Another baking at 150 °C for 30 min was conducted to further remove the solvent, enhance the contact of AgNWs at the junctions, and improve the conductivity of AgNW networks.[34] Next, liquid PDMS was cast on top of the AgNW pattern, degassed, and cured at 60 °C for 2 h. The patterned AgNWs were embedded just below the PDMS surface when it was peeled off the Si substrate. Conducive paste was finally applied onto the two ends of the AgNW/PDMS sensor to interconnect with other components.

*Fabrication Process of Artificial Skin*: The preparation of artificial skin follows the methods developed by Ito and Yamamoto et al.[17,18] Briefly, 0.3267 g sodium chloride (Sigma-Aldrich) and 1.743 g Agar (Sigma-Aldrich) were measured and mixed well in 56.25 g purified water, where purified water determines the water content, sodium chloride adjusts conductivity, and Agar allows for self-shaping and prevents water from separating. The mixture was then heated on a hotplate while being slowly stirred to prevent burning the agar. When the increase in viscosity of the mixture was observed, the mixture was removed from hotplate. Following that, 5.625 g polyethylene powder (Sigma-Aldrich) (adjusts the dielectric constant) and 1.382 g TX-151 (Balmar, LLC) (allows agar and polyethylene powder to be mixed and increases the viscosity) were added into the mixture and thoroughly mixed. Transferring the mixture into a petri dish or other molds finished the preparation of skin phantom.

*Fabrication Process of Multifunctional Chest Patch*: Briefly, a thin layer of liquid PDMS (Sylgard 184, Dow Corning) with the base to curing agent weight ratio of 10:1 was coated on a PET sheet followed by degassing and curing at 60 °C for 2 h. The masks for sensors were prepared by cutting the cured PDMS using a cutting tool (Silhouette CAMEO). AgNWs in ethanol (SLV-NW-90, Blue Nano) were drop-cast into the area defined by the mask. After drying the AgNWs on a hotplate with a temperature of 50 °C, the mask was removed. To render the AgNW into a stretchable manner, the AgNW area for the patch (except for the strain sensor electrodes) was encapsulated by PDMS with a base to curing agent weight ratio of 10:1. The AgNW area for strain sensor top and bottom electrodes was embedded by Dragon Skin FXO (Smooth-On, Inc.) with part A to part B ratio of 1:1 in weight. The area surrounding the AgNWs was covered by slacker (Smooth-On, Inc.) modified Dragon Skin FXO (Smooth-On, Inc.) to provide a self-adhesive and very compliant substrate. Curing at room temperature for 6 h was performed to cross-link the silicone. To finish the fabrication of strain sensors, liquid Ecoflex 0010 (Smooth-On, Inc.) serving as the dielectric for the capacitor was used to sandwich the AgNW/Dragon Skin FXO bottom electrode on the patch and the top electrode prepared separately. The patch was cured at room temperature for another 6 h. A line was cut between the connecting pads for the top and bottom electrodes to help the strain sensor top electrode connect to the connecting pad on the back (the side on the skin). The sensor patch was then peeled off the PET substrate. The resulting self-adhesive patch can be readily placed onto the skin for the multifunctional sensing.

## Acknowledgements

S.Y. and A.M. contributed equally to this work. The authors gratefully acknowledge the financial support from the National Science Foundation through the ASSIST Engineering Research Center at NCSU (EEC-1160483). J.F.M. would like to thank Chris Lamb at Device Solutions for several in-depth discussions with students about board layout, antenna design, and flexible electronic construction techniques. Y.Z. would like to thank Dr. Bongmook Lee at NCSU for helpful discussions in the initial stage of this work.

Received: October 11, 2016
Revised: December 9, 2016
Published online:

[1] E. Berardesca, *Skin Res. Technol.* **1997**, *3*, 126.
[2] Y. Yamamoto, T. Yamamoto, *Med. Biol. Eng. Comput.* **1986**, *24*, 71.
[3] Ø. G. Martinsen, S. Grimnes, *Dermatology* **2001**, *202*, 87.
[4] S. Björklund, T. Ruzgas, A. Nowacka, I. Dahi, D. Topgaard, E. Sparr, J. Engblom, *Biophys. J.* **2013**, *104*, 2639.
[5] X. Huang, H. Cheng, K. Chen, Y. Zhang, Y. Zhang, Y. Liu, C. Zhu, S.-C. Ouyang, G.-W. Kong, C. Yu, Y. Huang, J. A. Rogers, *IEEE Trans. Biomed. Eng.* **2013**, *60*, 2848.
[6] R. C. Webb, A. P. Bonifas, A. Behnaz, Y. Zhang, K. J. Yu, H. Cheng, M. Shi, Z. Bian, Z. Liu, Y.-S. Kim, W.-H. Yeo, J. S. Park, J. Song, Y. Li, Y. Huang, A. M. Gorbach, J. A. Rogers, *Nat. Mater.* **2013**, *12*, 938.
[7] D.-H. Kim, N. Lu, R. Ma, Y.-S. Kim, R.-H. Kim, S. Wang, J. Wu, S. M. Won, H. Tao, A. Islam, K. J. Yu, T.-I. Kim, R. Chowdhury, M. Ying, L. Xu, M. Li, H.-J. Chung, H. Keum, M. McCormick, P. Liu, Y.-W. Zhang, F. G. Omenetto, Y. Huang, T. Coleman, J. A. Rogers, *Science* **2011**, *333*, 838.
[8] F. Xu, Y. Zhu, *Adv. Mater.* **2012**, *24*, 5117.
[9] S. Yao, Y. Zhu, *Adv. Mater.* **2015**, *27*, 1480.
[10] L. Song, A. C. Myers, J. J. Adams, Y. Zhu, *ACS Appl. Mater. Interfaces* **2014**, *6*, 4248.
[11] R. Ivanic, I. Novotny, V. Rehacek, V. Tvarozek, M. Weis, *Thin Solid Films* **2003**, *433*, 332.
[12] S. Yao, Y. Zhu, *JOM* **2016**, *68*, 1145.
[13] A. Cömert, M. Honkala, J. Hyttinen, *Biomed. Eng. Online* **2013**, *12*, 26.
[14] J. Webster, *Medical Instrumentation: Application and Design*, Wiley, Hoboken, NJ **2009**.
[15] H. P. Schwan, in *Proc. 16th Annual Int. Conf. IEEE*, IEEE, Baltimore, MD, **1994**.
[16] X. Huang, W.-H. Yeo, Y. Liu, J. A. Rogers, *Biointerphases* **2012**, *7*, 52.
[17] K. Ito, K. Furuya, Y. Okano, L. Hamada, *Electron. Commun. Jpn.* **2001**, *84*, 67.
[18] T. Yamamoto, K. Sano, K. Koshiji, X. Chen, S. Yang, M. Abe, A. Fukuda, in *Engineering in Medicine and Biology Society (EMBC), 2013, 35th Annual Int. Conf. IEEE*, IEEE, Osaka, Japan, **2013**.
[19] I. Van Reeth, A. Wilson, *Cosmet. Toiletries* **1994**, *109*, 87.

[20] Y. Su, V. Kravets, S. Wong, J. Waters, A. Geim, R. Nair, *Nat. Commun.* **2014**, *5*, 4843.
[21] H. N. Malhotra, in *Lymphedema: Presentation, Diagnosis, and Treatment*, Vol. *3*, (Eds: A. K. Greene, S. A. Slavin, H. Brorson), Springer, Switzerland **2015**, Ch. 13.
[22] C. M. Sheehy, P. A. Perry, S. L. Cromwell, *Biol. Res. Nurs.* **1999**, *1*, 30.
[23] S. M. Kleiner, *J. Am. Diet. Assoc.* **1999**, *99*, 200.
[24] J. Chan, S. F. Knutsen, G. G. Blix, J. W. Lee, G. E. Fraser, *Am. J. Epidemiol.* **2002**, *155*, 827.
[25] C. Van Mieghem, M. Sabbe, D. Knockaert, *Chest* **2004**, *125*, 1561.
[26] A. C. Myers, H. Huang, Y. Zhu, *RSC Adv.* **2015**, *5*, 11627.
[27] S. Yao, Y. Zhu, *Nanoscale* **2014**, *6*, 2345.
[28] A. Caduff, F. Dewarrat, M. Talary, G. Stalder, L. Heinemann, Y. Feldman, *Biosens. Bioelectron.* **2006**, *22*, 598.
[29] A. Caduff, E. Hirt, Y. Feldman, Z. Ali, L. Heinemann, *Biosens. Bioelectron.* **2003**, *19*, 209.
[30] M. van Dooren, J. H. Janssen, *Physiol. Behav.* **2012**, *106*, 298.
[31] A. Nakasone, H. Prendinger, M. Ishizuka, in *Proc. 5th Int. Workshop on Biosignal Interpretation*, Citeseer, Tokyo, Japan, **2005**.
[32] J. Di, S. Yao, Y. Ye, Z. Cui, J. Yu, T. K. Ghosh, Y. Zhu, Z. Gu, *ACS Nano* **2015**, *9*, 9407.
[33] J. Nuutinen, R. Ikäheimo, T. Lahtinen, *Physiol. Meas.* **2004**, *25*, 447.
[34] D. Langley, G. Giusti, C. Mayousse, C. Celle, D. Bellet, J.-P. Simonato, *Nanotechnology* **2013**, *24*, 452001.